Physica B 464 (2015) 17–27

Contents lists available at ScienceDirect

Physica B

journal homepage: www.elsevier.com/locate/physb

Effect of nanosilica on optical, electric modulus and AC conductivity of polyvinyl alcohol/polyaniline films

Somyia El-Sayed [a,b,*], Tarob Abel-Baset [b], Azza Abou Elfadl [b], Arafa Hassen [a,b]

[a] Physics Department, Faculty of Science and Education, Taif University, Kingdom of Saudi Arabia
[b] Physics Department, Faculty of Science, Fayoum University, 63514 El Fayoum, Egypt

ARTICLE INFO

Article history:
Received 1 January 2015
Received in revised form
14 February 2015
Accepted 18 February 2015
Available online 19 February 2015

Keywords:
Nanosilica
PVA/PANI film
Nanocomposite films
XRD
FTIR
Optical and dielectric properties

ABSTRACT

Nanosilica (NS) was synthesized by a sol–gel method and mixed with 0.98 polyvinyl alcohol (PVA)/0.02 polyaniline (PANI) in different amounts to produce nanocomposite films. High-resolution transmission electron microscopy (HR-TEM) revealed the average particle size of the NS to be ca. 15 nm. Scanning electron microscopy (SEM) showed that the NS was well-dispersed on the surface of the PVA/PNAI films. The Fourier transform infrared (FTIR) spectra of the samples showed a significant change in the intensity of the characteristic peak of the functional groups in the composite films with the amount of NS added. The absorbance and refractive index (n) of the composites were studied in the UV–vis range, and the optical energy band gap, E_g, and different optical parameters were calculated. The dielectric loss modulus, M'' and ac conductivity, σ_{ac}, of the samples were studied within 300–425 K and 0.1 kHz–5 MHz, respectively. Two relaxation peaks were observed in the frequency dependence of the dielectric loss modulus, M''. The behavior of $\sigma_{ac}(f)$ for the composite films indicated that the conduction mechanism was correlated barrier hopping (CBH). The results of this work are discussed and compared with those of previous studies of similar composites.

1. Introduction

Polyvinyl alcohol (PVA) has fascinating properties and a wide variety of applications owing to its high dielectric strength and good charge storage capacity. Both its optical and electrical properties depend on the type of filler used. PVA has also gained increasing attention for biomedical applications [1]. PVA has a carbon chain backbone with hydroxyl groups that can act as a source of hydrogen bonding to enhance the formation of polymer complexes [2]. Polyaniline (PANI) has emerged as one of the most promising polymers for its ease of preparation, good environmental stability, and controllable electrical and optical properties. PANI has, therefore, been extensively studied and applied in diverse areas such as secondary batteries, anticorrosive coating, anti-static packaging materials, conductive coatings, capacitors, rotating machines, biosensors, electrostatic dissipation, optoelectronics, and electro-inactive materials [3–5].

PANI is known for its excellent thermal and environmental stability but poor processibility owing to its insolubility and brittleness, which limits its commercial applications. PANI can be made more processable in composites formed with other water soluble polymers such as, poly (vinyl pyrrolidone) (PVA), poly (acrylic acid), and poly (styrene sulfonic acid), which are used as stabilizers [6]. The stability of PANI dispersions in PVA has been reported to increase with PVA content [7], and the physical properties of PVA/PANI show a definite dependence on the ratio of these two polymers [8]. This further indicates the possible optimization of the ratio of the two polymers in the matrix to improve their specific optical and dielectric properties.

Nanosized silica (NS) particles have found large-scale applications in many every-day consumer products, ranging from automobile tires to optical fibers and catalyst supports. It has been reported that NS can increase the hardness and scratch resistance of a coating without affecting its optical clarity [9]. NS particles can also effectively improve the physical properties of polymeric materials [10]. For instance, NS particles have been widely introduced into polymer coatings to improve their heat resistance, wear resistance, hardness, and optical properties [11,12]. Polymer nanocomposites are a group of materials in which nanoparticles are dispersed in a polymer matrix. Compared with those of the pure polymers, polymer nanocomposites have different physical and mechanical characteristics including modulus, strength, hardness, flammability, dimensional stability, electrical conductivity, thermal resistance, and moisture absorption, depending on the type and amount of nanoparticles used [13–18].

* Corresponding author at: Physics Department, Faculty of Science and Education, Taif University, Kingdom of Saudi Arabia.
E-mail address: somyia.elsayed@yahoo.com (S. El-Sayed).

http://dx.doi.org/10.1016/j.physb.2015.02.016
0921-4526/

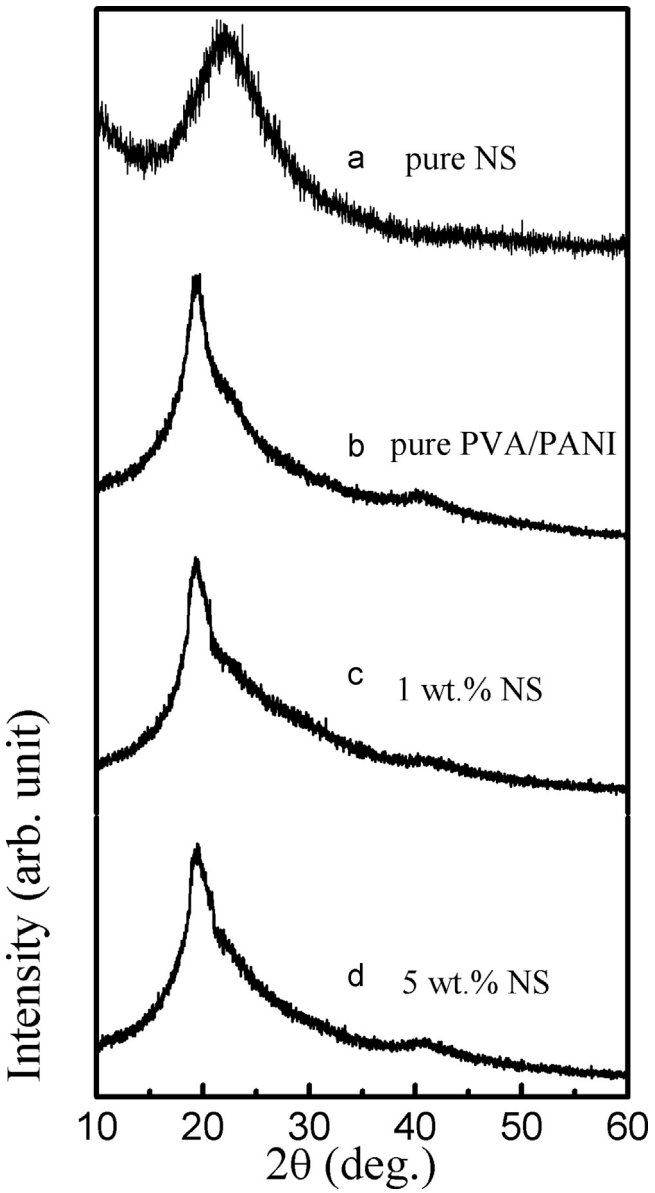

Fig. 1. XRD patterns measured at room temperature of (a) pure NS, (b) pure PVA/PANI film, (c) 1 wt% NS-doped PVA/PANI and (d) 5 wt% NS-doped PVA/PANI films.

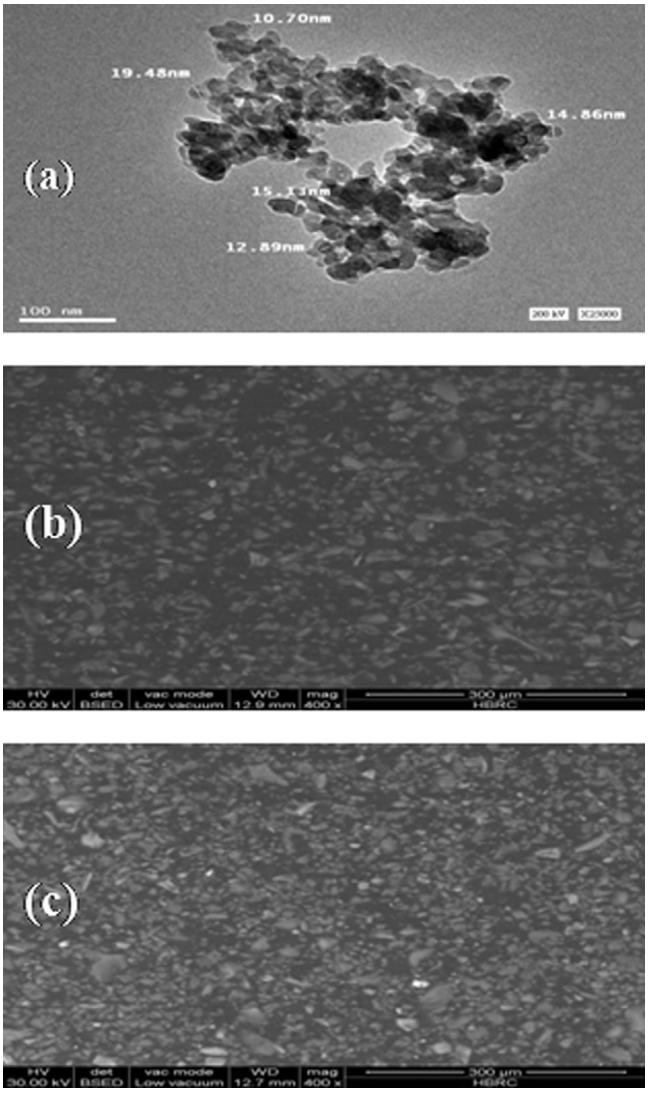

Fig. 2. (a) HR-TEM image of pure NS. SEM images of some selected NS-doped PVA/PANI films: (b) 1 wt% NS, and (c) 5 wt% NS.

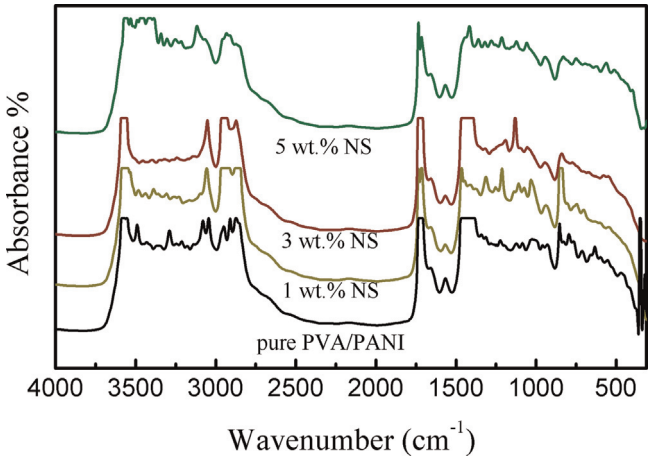

Fig. 3. FTIR spectra of pure PVA/PANI and PVA/PANI loaded with different NS content.

PANI–PVA–NiO (IPN) nanocomposite film containing nickel oxide nanoparticles uniformly dispersed in the polymer matrix has previously been successfully fabricated at room temperature [19]. Magnesium oxide (MnO_2)–loaded PANI/PVA thin films showed better response to ammonia and trimethyl ammine vapor than unloaded film [7]. X-ray diffraction (XRD) analysis revealed an increase in the crystallinity of these films with PVA concentration, with the possible interaction between PANI and PVA also indicated by Fourier transform infrared spectroscopy (FTIR). The non-ohmic I–V characteristics of the films suggest possible application in the field of device (particularly FET, etc.) fabrication [20].

PANI and its charge transfer complexes have been used as engineering materials owing to their unique electrochemical behavior, environmental stability, and high degree of processability. Extensive works on the preparation of electrically conductive PANI blends containing a polymeric matrix having desirable physical and mechanical characteristics represent a promising route to overcome the intractability of PANI. In this work, we aimed to improve the physical properties of PVA by adding 2 wt% PANI and then loading the mixture with different NS contents. The nanocomposite films were characterized by XRD and FTIR in addition to the study of their optical and dielectric properties.

Table 1
Observed characteristic vibrations from FTIR. The square brackets in this table refer to the references.

FTIR peak (cm^{-1})	Pure NS	Pure PVA	Pure PANI	Pure PVA/PANI	1 wt% NS-loaded PVA/PANI	3 wt% NS-loaded PVA/PANI	5 wt% NS-loaded PVA/PANI
N–H stretching			3306.64 [25]	3043.12	3054.69	3050.83	3116.40
C–N stretching			1568.99 [25]	1565.92	1569.77	1569.77	1569.77
O–H stretching		3565.5 [25]		3571.52	3575.38	3579.23	3559.95
C–H stretching		2921.6 [25]		2908.13	2938.98	2950.55	2935.13
Si–O–Si stretching	1140 [27–29]				1017.97	1130.08	1126.22
Si–OH stretching	960 [29,30]				944.95	944.95	944.94

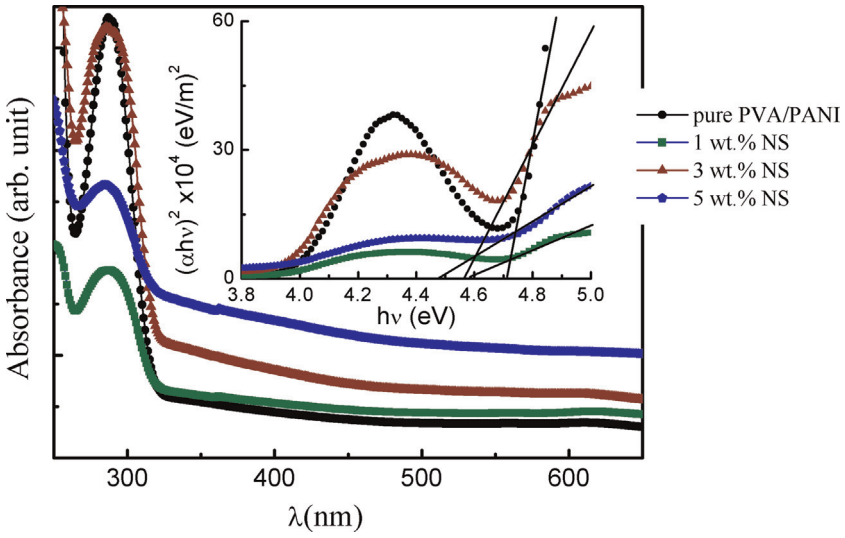

Fig. 4. The main frame represents UV–vis absorption spectra, and the inset shows the plots of $(\alpha h\upsilon)^2$ versus $h\upsilon$ for PVA/PANI film and PVA/PANI filled with NS.

Table 2
The direct energy band gap, E_g, Urbach energy, E_U, and various optical dispersion parameters of pure PVA/PANI and PVA/PANI loaded with different contents of NS.

Sample		E_g (eV)	E_U (eV)	E_d (eV)	E_o (eV)	n_∞	λ_o (nm)	$S_o \times 10^{12}$ (m^{-2})
NS (wt%)	PVA/PANI (wt%)							
0	100	4.72	0.39	10.90	3.69	1.15	314.14	3.27
1	99	4.60	0.33	10.28	4.02	1.17	318.97	3.63
3	97	4.57	0.37	10.84	7.64	1.29	314.77	6.70
5	95	4.48	0.29	13.66	18.53	1.51	283.03	15.90

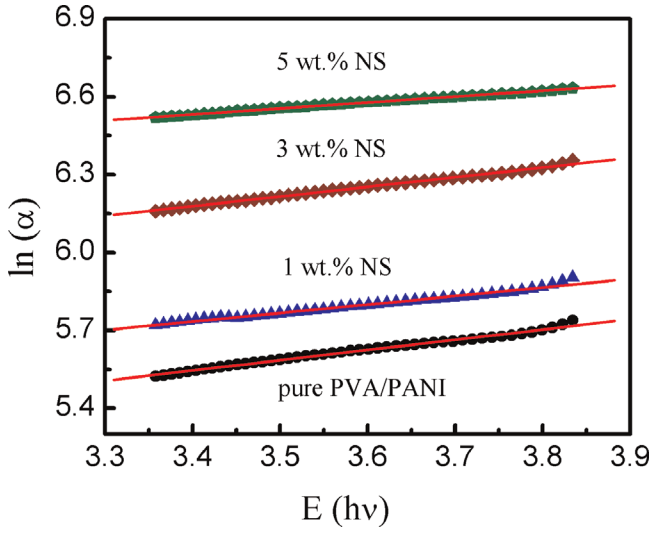

Fig. 5. Plots of $\ln(\alpha)$ versus $h\upsilon$ of pure PVA/PANI film and that loaded with different ratios of NS. The solid lines in are the fittings according to Eq. (3).

2. Experimental

Silica nanoparticles were synthesized via a sol–gel method. A desired amount of sodium silicate (Na_2SiO_3, Sigma-Aldrich) was dissolved in distilled water under stirring for 15 min, and then precipitated using dilute hydrochloric acid. The precipitate was filtered and washed several times with distilled water until complete removal of sodium chloride from the precipitate, and then the precipitate was dried overnight. The synthesized SiO_2 nanoparticles were added to PVA/PANI in different concentrations (1, 3, and 5 wt%) according to the relation:

$$x(\text{wt\%}) = \left(\frac{w_f}{w_p + w_f}\right) \times 100 \quad (1)$$

where w_f and w_p represent the weights of SiO_2 and PVA/PA, respectively. The nanocomposite films were prepared as follows: 1.0 g of the PVA/PANI mixture was dissolved in 25 mL distilled water under stirring until a clear solution was obtained. The required mass of the prepared NS particles was added to the solution under ultrasonic stirring at RT for 30 min to prevent the agglomeration of the nanoparticles. The obtained mixtures were then cast into Petri dishes and left to dry in air at RT for 24 h. Finally, the

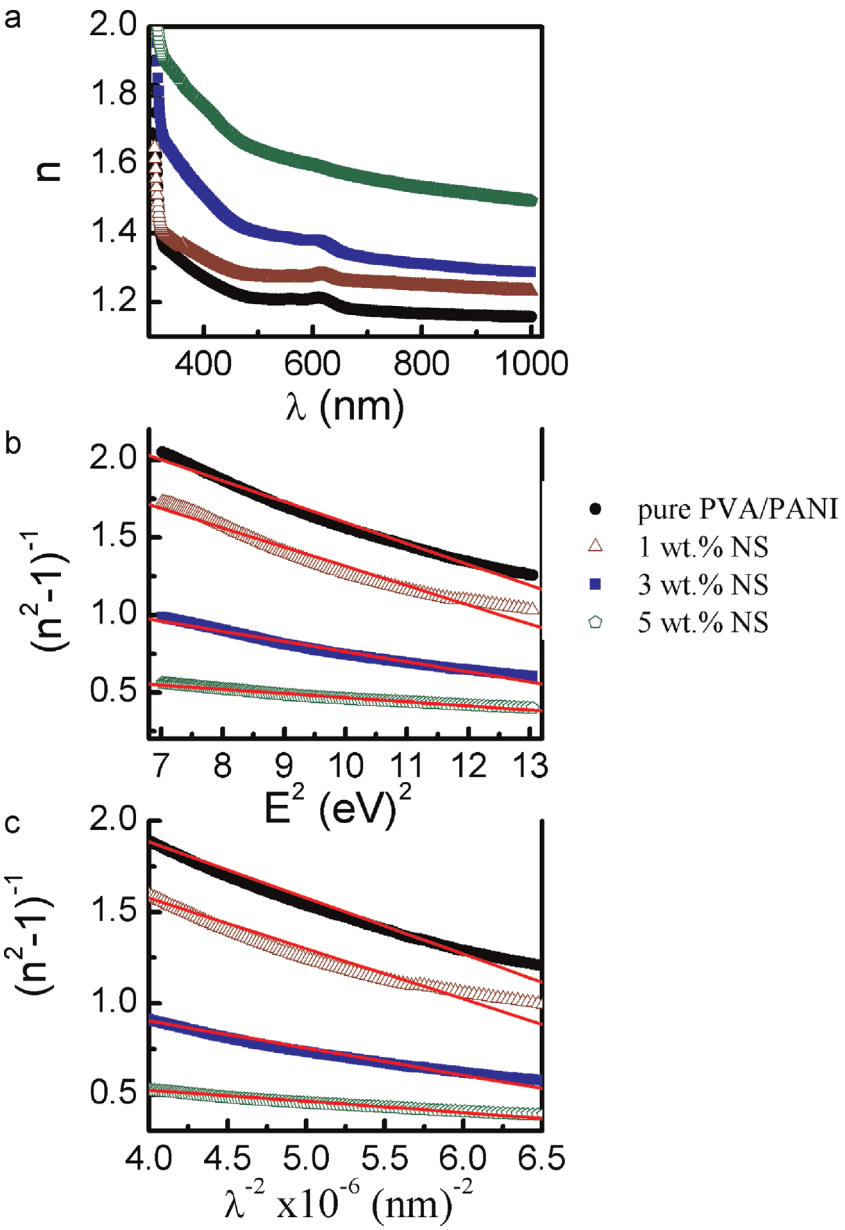

Fig. 6. (a) Dependence of refractive index (n) on wavelength (λ), (b) Plots of $(n^2-1)^{-1}$ against $(E)^2$, and (c) $(n^2-1)^{-1}$ versus λ^{-2} for pure PVA/PANI and PVA/PANI loaded with NS. The solid red lines in (b) and (c) are the linear fitting according to Eqs. (5) and (6), respectively. (For interpretation of the references to color in this figure legend, the reader is referred to the web version of this article.)

films were peeled off from the Petri dishes and care was taken to obtain homogenous samples with the same thickness (≈ 0.1 mm). It was not possible to prepare composites with higher (>5 wt%) NS loadings because of agglomeration.

X-ray diffraction (XRD) analysis of the samples was performed using a Rigaku miniflex diffractometer with CuK_α radiation ($\lambda = 1.5406$ Å). High-resolution transmission electron microscopy (HR-TEM; JEM 2100, JEOL, Japan) was used to determine the particle size of the as-synthesized nanosilica. Scanning electron microscopy (SEM; Inspect S, FEI, Holland) images were taken of the pure PVA/PANI and the nanocomposite films. The FTIR spectra of all samples were recorded using a Shimadzu 8201 PC in the range of 4000–400 cm^{-1}. The spectra were obtained with a resolution of 1.0 cm^{-1} and accuracy better than ± 3 cm^{-1}. Optical characterization was carried out using a Shimadzu UV-3600 UV–vis–NIR spectrophotometer in the wavelength range 200–850 nm with an accuracy of ± 0.2 nm. The temperature and frequency dependence of the dielectric characterization was carried out using an LCR meter (model 3532, HIOKI, Ueda, Nagano, Japan), with a capacitance measurement accuracy on the order of 0.0001 pF. The temperature was measured with a T-type thermocouple having an accuracy of ± 1 °C. The dielectric constant, ε', of each sample was calculated as $\varepsilon' = dC/\varepsilon_0 A$, where C is the capacitance, d is the thickness of the sample, ε_0 is the permittivity of free space, and A is the cross-sectional area of the sample. The dielectric loss, ε'', is calculated from ε' tan δ, where tan δ is $\varepsilon'/\varepsilon''$. The total ac conductivity (σ_t) was obtained using $\sigma_t = 2\pi f \varepsilon_0 \varepsilon''$. The ac conductivity ($\sigma_{ac}$) was corrected from the low-frequency conductivity (σ_{dc}) as given in Eq. (9).

3. Results and discussion

3.1. Characterization

The XRD patterns of nanosilica (NS), pure PVA/PANI, and the nanocomposite films are shown in Fig. 1(a–d). The amorphous

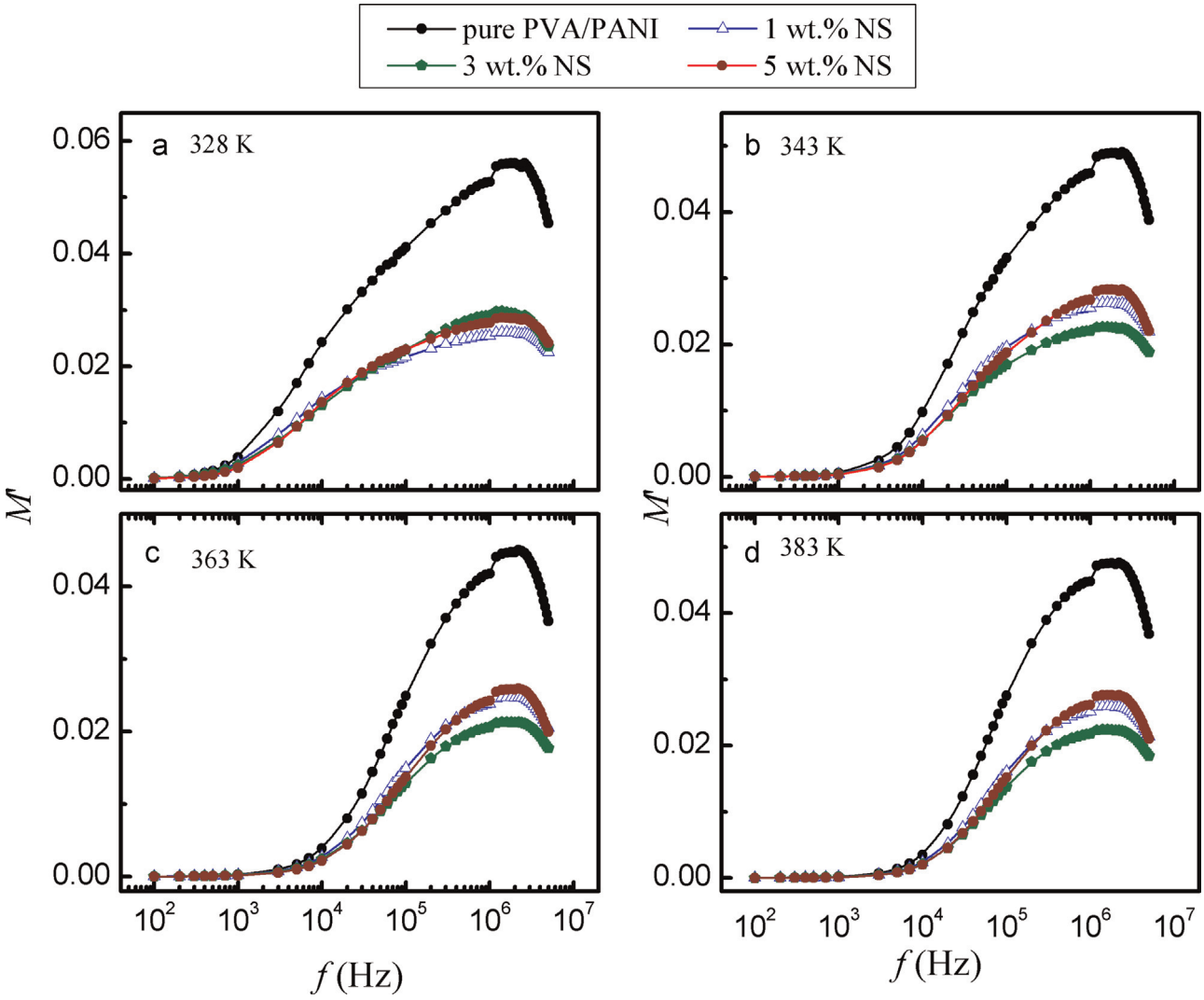

Fig. 7. Frequency dependence of M' for pure PVA/PANI film and that loaded with different NS content at different temperatures: (a) 328 K, (b) 343 K, (c) 363 K, and (d) 383 K.

nature of the nanosilica was clearly observable in Fig. 1(a), consistent with previous reports [21,22]. The observed maximum intensity diffraction peak of pure PVA/PANI and that loaded with NS was $2\theta = 19.5°$ which corresponded to a d spacing of 4.5501 Å and reflection plane (101) for the host material (PVA), similar to that reported in Ref. [23]. Another small peak observed around $2\theta = 40.6°$ indicated the presence of the typical semicrystalline structure of PVA [24]. No clear peaks were indexed around $2\theta = 23.44°$ for PANI as reported in Ref. [25]. This means that the PANI in the samples exhibited an amorphous behavior.

The as-prepared NS were imaged by HR-TEM to determine their crystal size. It can be seen from Fig. 2(a) that the NS was well defined and ranged from 10.7 to 19.5 nm in size. The average particle size was about 15 nm. This indicates that our synthesis process was a suitable method for obtaining NS. Fig. 2(b–c) shows the SEM images of selected nanocomposite films, in which it can be seen that there was a good dispersion of NS on the surface of the PVA/PANI.

FTIR spectroscopy is very sensitive to the formation of hydrogen bonds [26] and can be used to identify interaction in polymer composites. Fig. 3 shows the FTIR absorption spectra obtained for pure PVA/PANI and that loaded with 1, 3, and 5 wt% NS. The observed strong bands are summarized in Table 1. There are two main characteristic bands for pure PVA [25,26]; the first at 3565.5 cm^{-1} is caused by O–H stretching vibrations of the hydroxyl groups of PVA. The second band is at 2921.6 cm^{-1} and arises from C–H stretching. These bands were observed for our investigated films. Except for 5 wt% NS-loaded PVA/PANI, there was a regular shift of the O–H stretching vibration to higher wavenumber with NS loading. Similarly, C–H stretching was enhanced for the nanocomposite films compared with the pure PVA/PANI film. Two characteristic bands are reported for PANI [25]; the C–N stretching band at 1568.99 cm^{-1} was the same for all investigated samples. The second, N–H stretching, appears around 3306.64 cm^{-1} and was shifted to lower wavenumber in the pure PVA/PANI and that loaded with different NS content. Two other observed bands that were characteristic of NS particles appeared at 1140 cm^{-1} [27–29], attributed to Si–O–Si stretching, and 960 cm^{-1} [27,30], attributed to Si–OH stretching, in the spectra of the NS-loaded PVA/PANI films. Moreover, the peaks observed around 640 and 559 cm^{-1} were a clear indication of PVA–PANI crosslinking because these bands do not appear in the spectra of either pure PVA or pure PANI [20].

As seen from Fig. 3 and Table 1, the FTIR bands of NS-loaded PVA/PANI were not modified drastically from those of the pristine film. This indicates that the PVA/PANI film was not damaged by the addition of the NS. Also, the absorbance peaks showed a regular increase in the intensity with NS particle loading. This was caused

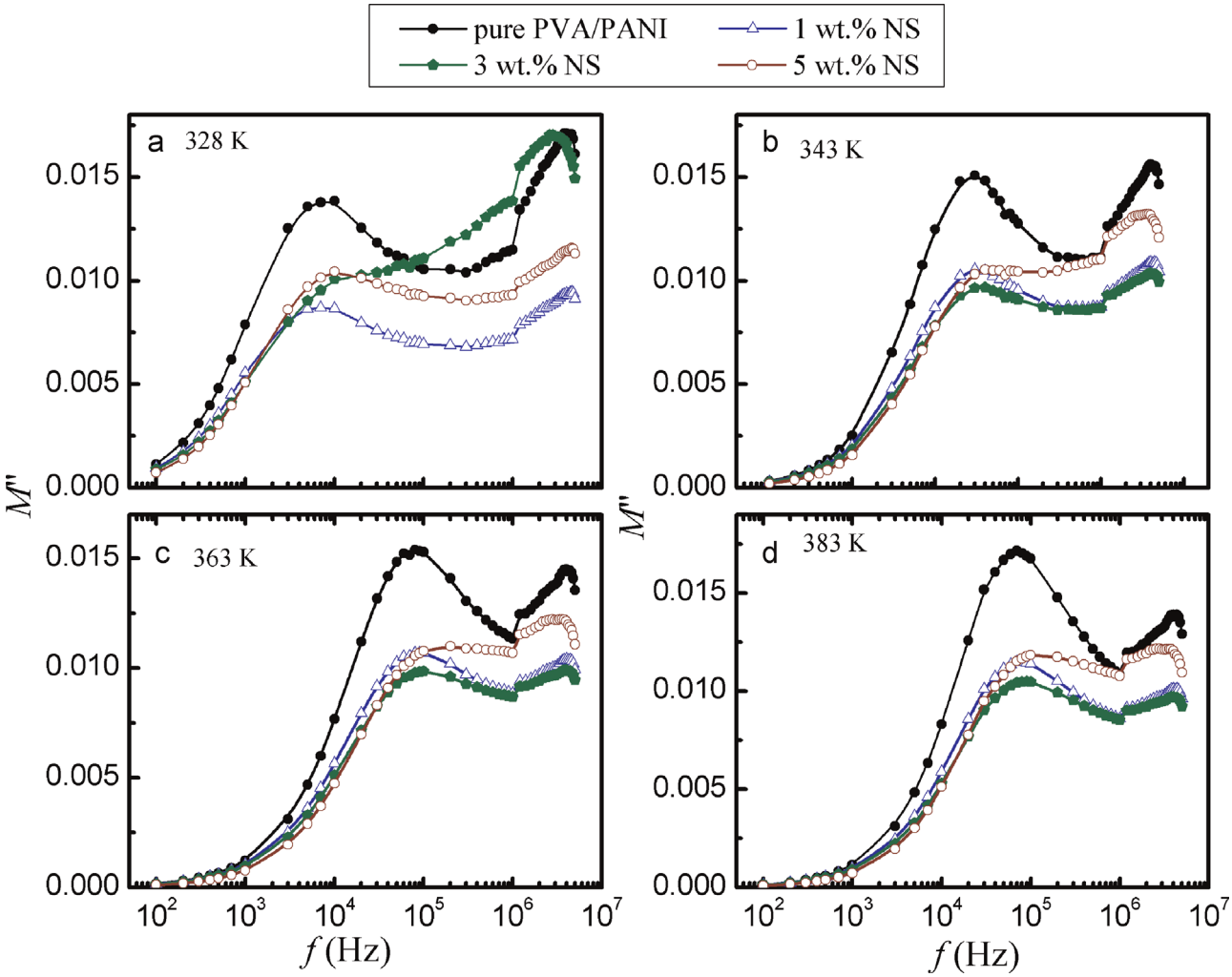

Fig. 8. Frequency dependence of M'' for pure PVA/PANI and PVA/PANI loaded with different NS ratio at different temperatures: (a) 328 K, (b) 343 K (c) 363 K and (d) 383 K.

by the formation of bonds between the constituents of the composite materials.

3.2. Optical properties

UV–vis absorption spectroscopy is a direct and simple method of probing the band structure of materials. The UV–vis absorption spectra of pure PVA/PANI and PVA/PANI loaded with NS are presented in Fig. 4. The absorbance of the films changed with increasing NS content in the PVA/PANI matrix. An absorption band at ~280 nm assigned to the π–π* transition in PVA was observed for both the pure and NS-loaded PVA/PANI films [31–33]. The intensity of this band was dependent on the amount of NS in the nanocomposite films. Another small peak around 600 nm was observed for the pure PVA/PANI film and those loaded with 1 and 3 wt% NS. This peak can be attributed to the formation of charge transfer complexes. The direct optical energy band gap (E_g) of the films was determined from their UV–vis spectra according to the frequency dependence of the absorption coefficient, α, (where α=absorbance/film thickness) and using Tauc's relation [34–37]:

$$\alpha h\upsilon = B\left(h\upsilon - E_g\right)^r \tag{2}$$

where $h\upsilon$ is the incident photon energy, approximated to $h\upsilon = 1240/\lambda$, B is a constant, and r is assumed to be 2 for allowed indirect transitions [38]. A plot of $(\alpha h\nu)^2$ versus $h\nu$ at *RT* enables the estimation of E_g by extrapolating the linear part of $(\alpha h\nu)^2$ to zero, as shown in the inset of Fig. 4. The obtained E_g values are listed in Table 2. E_g decreased to 4.48 eV as the NS content increased to 5 wt%. Similar behavior has been reported for other composite polymers [31,39,40]. This decrease in E_g is attributed to the creation of localized states in the band gap as a result of NS loading.

The absorption coefficient near the fundamental absorption edge is exponentially dependant on $h\upsilon$ and obeys the empirical Urbach relation. The Urbach energy (E_U) can be calculated using the following equation [41]:

$$\alpha = \alpha_o \exp\left(\frac{h\upsilon - E_I}{E_U}\right) \tag{3}$$

where E_I and α_o are constants. E_U values were calculated from the slopes of the graphs shown in Fig. 5 using the relationship $E_U = (d\ ln\alpha/d\ h\upsilon)^{-1}$, and are given in Table 2. The E_U values of the PVA/PANI films decreased with NS content. E_U changed to become similar to E_g, which may have been caused by the disorder of the PVA/PANI matrix being increased by NS loading. This decrease would lead to a redistribution of states from the band to tail, allowing a large number of possible band-to-tail and tail-to-tail transitions [42]. Moreover, the decrease in the optical band gap, E_g, and the increase of σ_{ac} indicated an expected consistency between the ac conductivity and optical

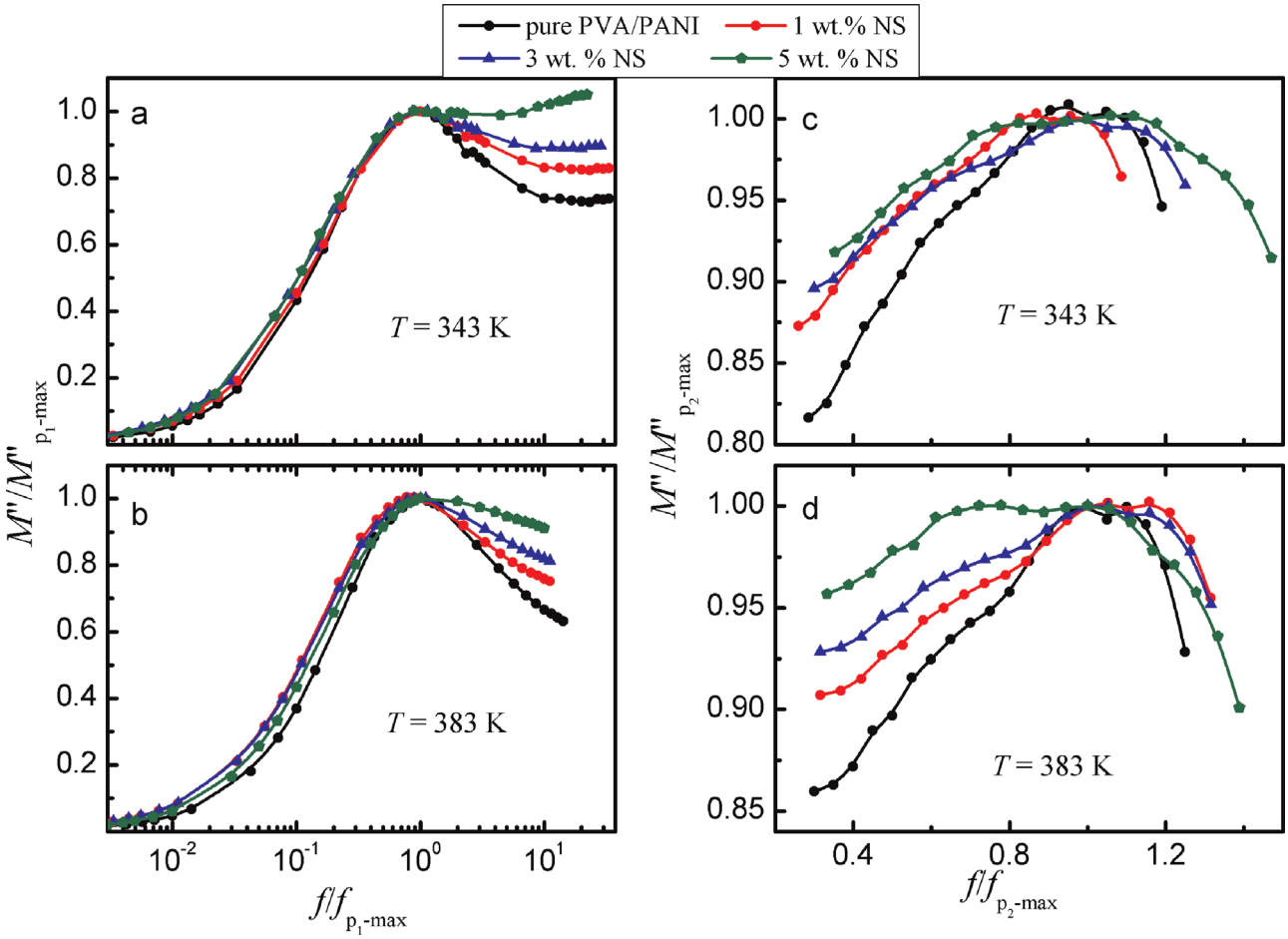

Fig. 9. Master curves for pure PVA/PANI and that loaded with NS scaled by the first peak maximum (α-peak, i.e. p_1) and position at (a): 343 K and (b) 383 K. Master curves pure PVA/PANI film and PVA/PANI loaded with NS scaled by the second peak (p_2) maximum and position at: (c) 343 K and (d) 383 K.

measurements.

One method of calculating the refractive index (n) of a film is to use the reflectance (R) and extinction coefficient, k, ($k=\alpha\lambda/4\pi$) as follows [43]:

$$n = \left[4R/(1-R)^2 - k^2\right]^{1/2} + [(1+R)/(1-R)] \quad (4)$$

where n is the real part of the complex refractive index given by $\tilde{n} = n + ik$, and R is the reflectance calculated from the absorbance (A) and transmission (T) spectra using the relation; $R = 1 - \sqrt{T \exp(A)}$ [43]. Fig. 6(a) shows the refractive index distributions of the pure PVA/PANI film and that loaded with NS particles. The n of the PVA/PANI film increased regularly with the NS content, consistent with results observed for PVC/CdO [31] and PVC/Cr_2O_3 [44] nanocomposites. The physical properties of a material depend strongly on its internal structure, including packing density and molecular weight distribution. The increased n of PVA/PANI after embedding NS may have been caused by the formation of intermolecular hydrogen bonds between the oxygen atoms of NS and the adjacent hydrogen atoms of PVA or PANI. This increase in n may allow these materials to be used as an anti-reflection coating for solar cells, or as high-refractive-index lenses. A small peak was observed in n ($h\nu$) in the pristine film and those loaded with 1 and 3 wt% NS.

From the normal dispersion behavior of n with λ, various dispersion parameters can be calculated within selected absorbance bands on the basis of the single oscillator model developed by DiDomenico and Wemple [45,46]:

$$n^2 = 1 + \frac{E_d E_o}{E_o^2 - (h\nu)^2} \quad (5)$$

where E_d is a measure of the strength of the interband optical transitions while E_o is the average excitation energy for the electronic transitions. Both E_d and E_o can be obtained from the intercept and slope of the linear fit of $(n^2-1)^{-1}$ against E^2, as depicted in Fig. 6(b). The determined values of E_d and E_o are listed in Table 2. The variation of n with λ can be expressed as [47]:

$$\frac{n_\infty^2 - 1}{n^2 - 1} = 1 - \left(\frac{\lambda_o}{\lambda}\right)^2 \quad (6)$$

where n_∞ is the long-wavelength refractive index and λ_o is the average interband oscillator wavelength. The parameters n_∞, λ_o, and S_o (average oscillator strength; $S_o = (n_\infty^2 - 1)/\lambda_o^2$) were obtained from the slope and intercepts of the $(n^2-1)^{-1}$ versus λ^{-2} curves presented in Fig. 6(c). The values of these parameters are also given in Table 2. The optical parameters of PVA/PANI were changed by the incorporation of NS into the polymer matrices. This suggests that the optical constants of the nanocomposite films could be changed by their NS content. The quantitative measurement of these parameters may assist in tailoring and modeling the properties of such nanocomposites for use in optical components and devices.

3.3. Electric modulus

In composite polymeric materials, the presence of interfaces gives rise to interfacial polarization, or the Maxwell–Wagner–

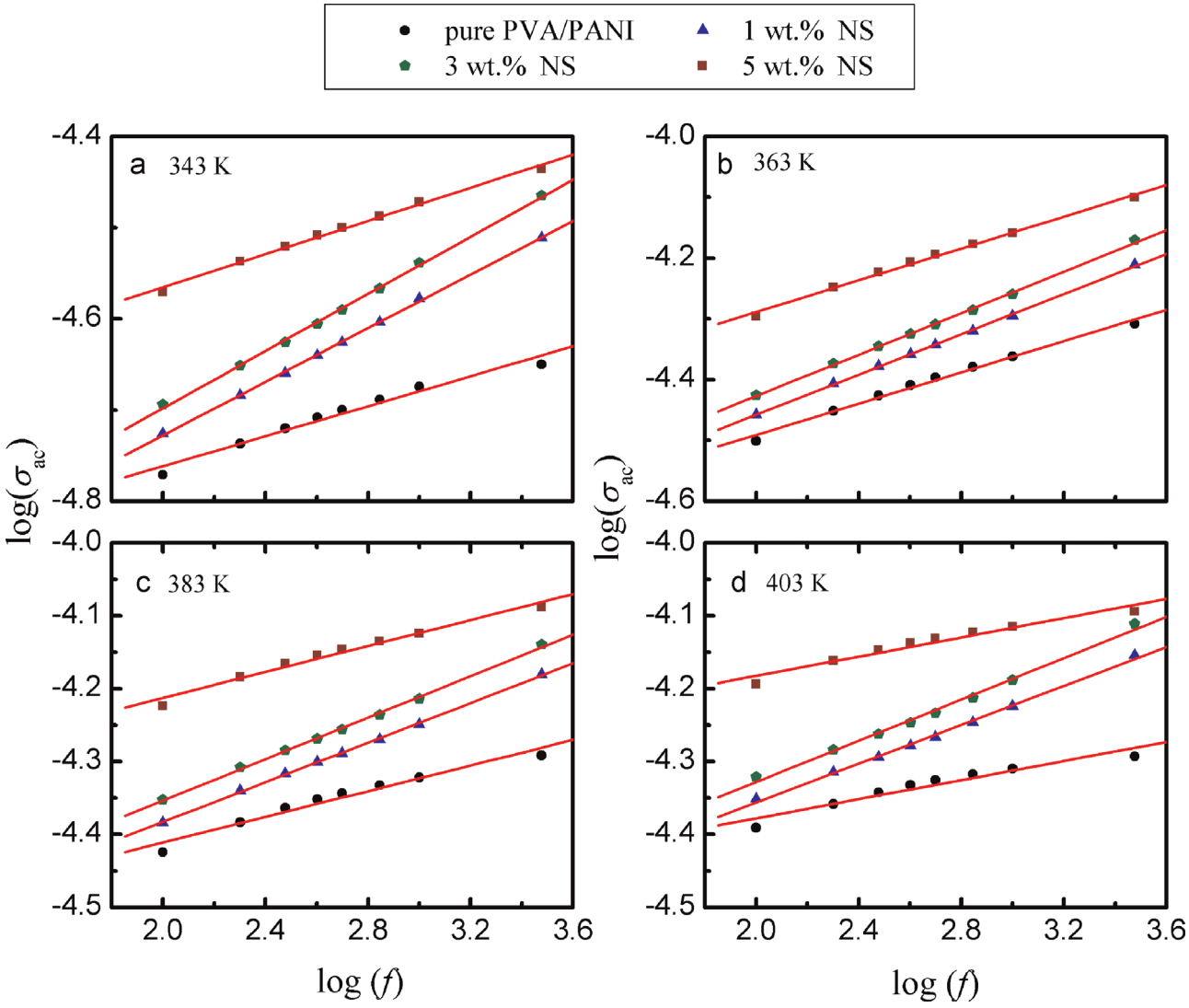

Fig. 10. Frequency dependence of σ_{ac} for: (a) pure PVA/PANI films and those loaded with different NS content at different temperatures: (a) 343 K, (b) 363 K, (c) 383 K and (d) 403 K. The solid red lines show the fits to Eq. (9). (For interpretation of the references to color in this figure legend, the reader is referred to the web version of this article.)

Table 3
The values of the exponent, *s*, for pure and NS-loaded PVA/PVNI at different temperatures according to the fitting of Eq. (9).

Sample		312 K	323 K	343 K	383 K	403 K
NS (wt%)	PVA/PANI (wt%)					
0	100	0.365	0.207	0.085	0.082	0.065
1	99	0.369	0.193	0.147	0.136	0.133
3	97	0.402	0.143	0.157	0.142	0.142
5	95	0.434	0.104	0.091	0.089	0.066

Sillers (MWS) effect. This effect appears in heterogeneous media because of the accumulation of charges at the interfaces, and is why the dielectric permittivity becomes high at low frequencies and high temperatures. To overcome the difficulty of experimentally observing the interfacial polarization, the modulus formulism can be used to analyze the electrical conductivity of an ionic polymeric material [48]. In addition, the modulus formalism can be used to suppress the signal intensity associated with the electrode polarization, to emphasize small features at high frequencies. The recorded dielectric data can be expressed in terms of the complex electric modulus (M^*), which is defined as the inverse of the complex permittivity (ε^*):

$$M^* = \frac{1}{\varepsilon^*} = \frac{\varepsilon'}{\varepsilon'^2 + \varepsilon''^2} + i\frac{\varepsilon''}{\varepsilon'^2 + \varepsilon''^2} \quad (7)$$

or

$$M^* = M' + iM'' \quad (8)$$

where M' and M'' are the real and imaginary parts of the electric modulus, respectively.

The frequency dependence of the real part of the dielectric modulus (M') of the pristine PVA/PANI and nanocomposite films at various temperatures are plotted in Fig. 7(a–d). It is clear that the values of M' increased with frequency and exhibited an S-shaped trend. This S-shaped dispersion of M' is typical of ionic materials [49]. The near zero M' values at low frequency indicate the removal of the electrode polarization for the investigated samples. This result suggests that electrode polarization plays a role at high temperatures and low frequencies. The NS within the PVA/PANI matrices influenced the polarization and correspondingly the electrical conductivity of the films.

From a physical point of view, the electrical modulus corresponds to the relaxation of the electric field in the materials when

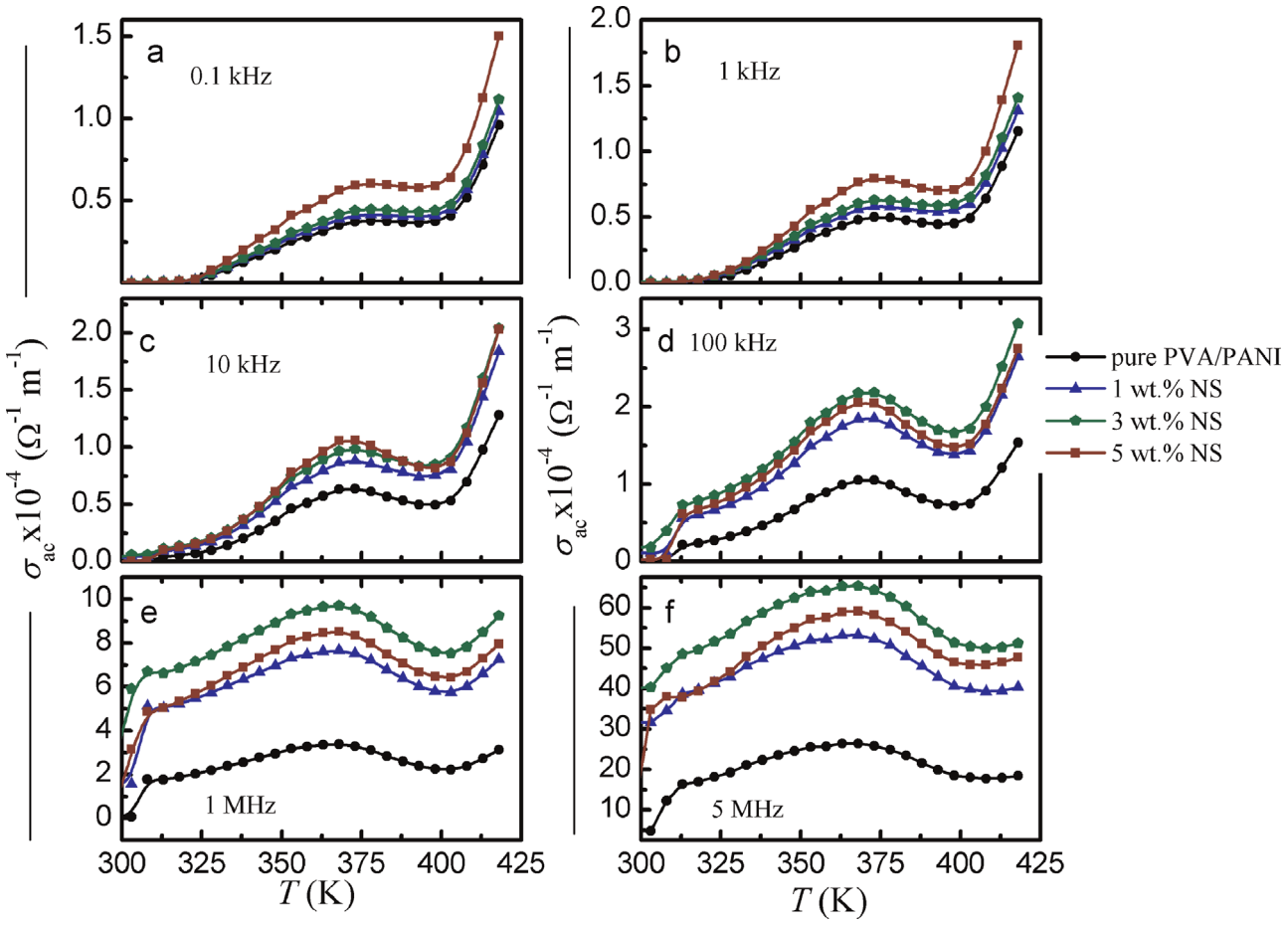

Fig. 11. The temperature dependence of ac conductivity, σ_{ac}, of pure PVA/PANI film and that loaded with different NS content at different selected frequencies.

the electric displacement remains constant. Fig. 8(a–d) shows the plots for the imaginary part (M'') as a function of frequency at various temperatures for all investigated samples. The two peaks observed in the plot M'' indicate relaxation processes; the first was attributed to α-relaxation because of dipole orientation, while the second can be ascribed to side group motions or conformational changes in side groups similar to that reported for poly (3-hydroxy) butyrate [50]. The position of the first peak (α-relaxation) shifted toward higher frequency with increasing temperature. This relaxation peak was observed for all investigated samples within the studied frequency range. The second relaxation peak of $M''(f)$ moved slightly toward lower frequency with temperature. The frequency range peak maximum ($M_{m''}$) determines the range in which charge carriers are mobile over long distances. At frequencies above the peak maximum, the carriers are confined to potential wells and, therefore, are mobile for only short distances.

3.3.1. Frequency temperature superposition (FTS)

The frequency temperature superposition (FTS) principle describes the microscopic mechanisms under study in many electrical and mechanical systems. When investigating the spectral shapes of these systems, it is possible to force the data corresponding to different temperatures to fall on a single master curve, which indicates some similarity in the physical mechanisms that underlie various materials. This behavior also demonstrates that the microscopic mechanisms of various systems are independent of temperature [51]. For examples, inorganic solids, glasses, semiconductors, and polymers have been found to follow FTS [52,53]. Fig. 9(a–d) presents the dielectric spectra of the normalized-imaginary part of the electric modulus, $M''/M''_{j\text{-max}}$, as a function of the normalized-frequency $f/f_{j\text{-max}}$, where j refers to first peak (p_1) and second peak (p_2) for all samples, measured at two different temperatures. As seen from the figure, FTS applies to the lower side of the first peak only, and does not work well for the full spectrum at high frequencies. This means that the master curve for all of the films falls below $f/f_{j\text{-max}}$ at higher frequencies. This behavior suggests different relaxation mechanisms in these samples for this specific range of temperatures and frequencies.

3.4. Ac conductivity analysis

The frequency dependence plots of ac conductivity (σ_{ac}) measured at different temperatures are shown in Fig. 10(a–d). σ_{ac} was found to increase with frequency and temperature. The temperature dependence arose from a combination of inhomogeneity and microscopic disorder. At a particular T for a disordered semiconductor, σ_{ac} obeys the following relation [54,55]:

$$\sigma_{ac}(f) = \sigma_t - \sigma_{dc} = 2\pi B f^s \tag{9}$$

where σ_{dc} is the low-frequency conductivity, σ_t is the total conductivity, s is a universal exponent, and B is a pre-exponential factor. The dc conductivity is subtracted by extrapolating σ_t (f) to $f \rightarrow 0$. Various theoretical models for ac conductivity have been proposed to explain experimental observations of complex systems. In the electron tunneling model, s is independent of T but dependent on f. In the case of small polaron tunneling, s increases with of T. The correlated barrier hopping (CBH) model [56] predicts a decrease in s with temperature. In the CBH model, the charge carrier hops between sites over the potential barrier separating them. To identify the dominant conduction mechanism,

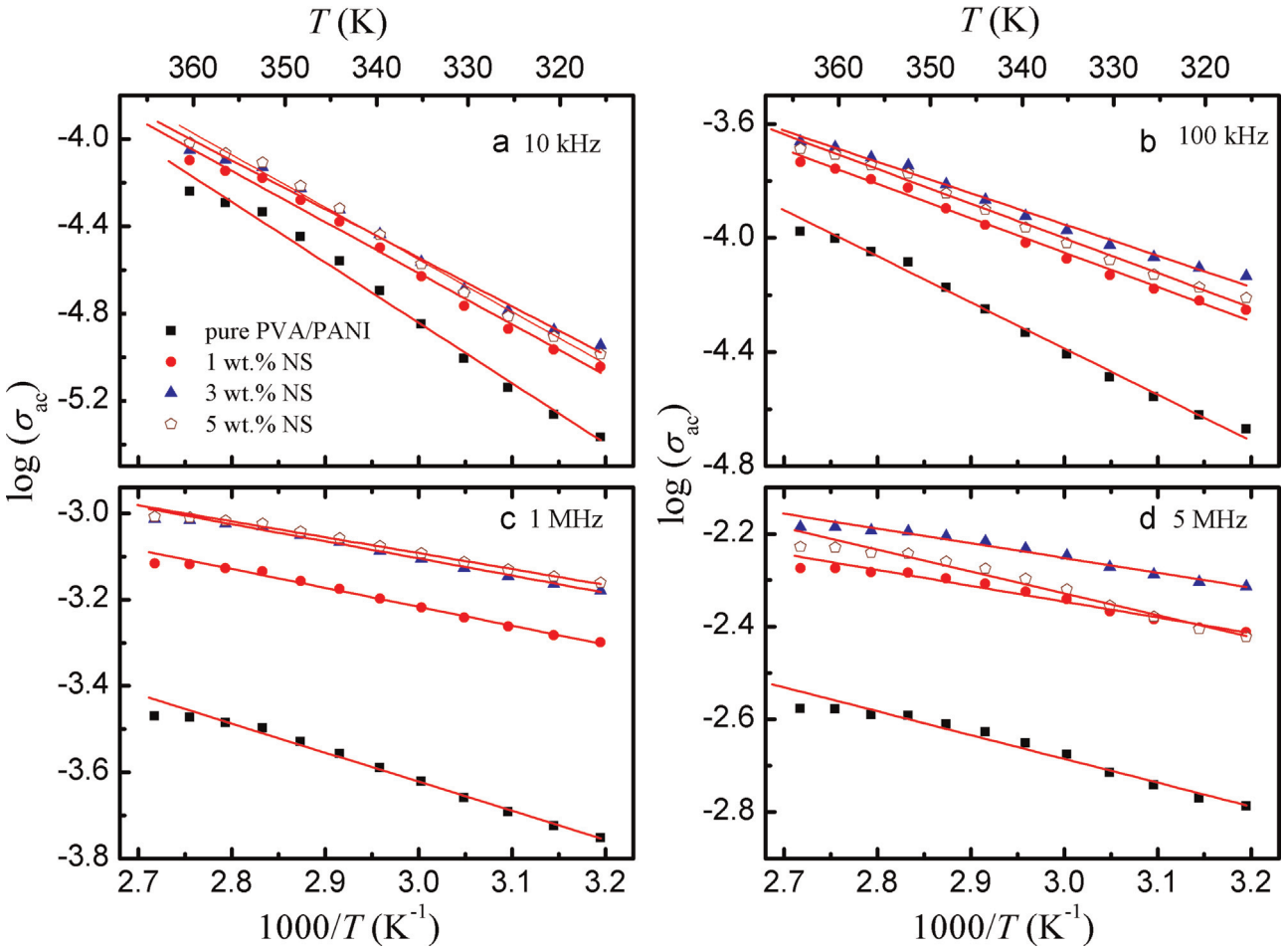

Fig. 12. The temperature dependence of ac conductivity, σ_{ac}, of pure PVA/PANI film and that loaded with different NS content at different frequencies; (a) 10 kHz, (b) 100 kHz (c) 1 MHz, and (d) 5 MHz. The solid red lines show the fit according to Eq. (10). The top of the upper frames shows the corresponding T range to 1000/T. (For interpretation of the references to color in this figure legend, the reader is referred to the web version of this article.)

Table 4
Activation energies of pure PVA/PANI and PVA/PANI films loaded with different NS content according to the fit of Arrhenius relation (Eq. (10)) within the temperature range of 313–363 K.

Sample	f= 10 kHz E (eV)	100 kHz E (eV)	1 MHz E (eV)
Pure PVA/PANI	0.238	0.139	0.058
1 wt% NS	0.202	0.103	0.038
3 wt% NS	0.192	0.094	0.034
5 wt% NS	0.206	0.105	0.032

we considered the frequency dependence of σ_{ac} within the experimental frequency range (0.1–3 kHz), as shown in Fig. 10(a–d). The results yielded straight lines with different slopes (i.e., different s). Table 3 shows the values of s for the pure and NS-loaded PVA/PANI films at various temperatures. Because s decreased with increasing temperature, we believe the conduction mechanism to be CBH within the studied frequency range.

The temperature dependence of σ_{ac} for the pure PVA/PANI film and that loaded with NS at certain representative frequencies is shown in Fig. 11(a–f). σ_{ac} increased with frequency and exhibited a peak at around 365 K, attributable to the crystalline region or α-relaxation. This peak broadened and shifted to lower temperature with increasing frequency. The effect of NS on the mixture of PVA and PANI was pronounced at higher frequencies, and the NS clearly increased the conductivity of the PVA/PANI polymers. The temperature dependence of the conductivity presented as log(σ_{ac}) versus the reciprocal temperature at selected frequencies is shown in Fig. 12(a–d). Within the temperature range (313 K ≤ T ≤ 363 K), ac conductivity is thermally activated according to the Arrhenius relation:

$$\sigma_{ac} = \sigma_o \exp(-E/kT) \quad (10)$$

where σ_o is the pre-exponential factor and E is the activation energy. The increase of σ_{ac} with temperature may have been caused by an increase in the absorbed energy, which leads to an increase in the number of charge carriers that contribute to the conduction process. This reveals that the conduction mechanism could be a hopping one. Also, the variation of the conductance with temperature can be attributed to a combined effect of the change in the conductance with temperature and to the nature of the trap distribution inside the polymer networks. The value of E was calculated and listed in Table 4. The value of E decreases as the frequency increases and is slightly dependent on the NS content.

4. Conclusions

Nanosilica (NS) particles having an average particle size of 15 nm were successfully prepared using a sol–gel method and loaded into pure PVA/PANI film at 1, 3, and 5 wt%. SEM images showed that the prepared films of both pure PVA/PANI and that loaded with NS were homogenous. There was no pronounced effect of the NS on the crystal structure of the PVA/PANI matrix. FTIR

spectroscopy confirmed the formation of PVA/PANI matrix as well as NS-(PVA+PANI) nanocomposite films. The addition of the NS nanoparticles to the PVA/PANI films modified their optical properties considerably. The direct optical energy band gap showed a shift from 4.72 to 4.48 eV upon addition of NS nanoparticles. The refractive index of pure PVA/PANI was observed to increase with NS content. The optical dispersion constants of the films also changed with NS addition. These results reveal that the present NS-loaded PVA/PANI films may be suitable for application in optical devices. Our measurements of the frequency dependence of the dielectric modulus of the pure and NS-loaded PVA/PANI films revealed two relaxation processes in the temperature and frequency ranges studied. The first is α-relaxation, which we attribute to micro-Brownian motion of the polymer backbones in the amorphous or crystalline regions of PVA. The second can be attributed to side group motions or conformational changes in side groups of the polymeric matrices. The ac conductivity σ_{ac} of the investigated samples also revealed that CBH is the most probable conduction mechanism for both the pure and NS-loaded PVA/PANI films. Moreover, the temperature dependence of the ac conductivity was found to be thermally activated within 313–363 K.

References

[1] C.H. Cholakis, W. Zingg, M.V. Seffon, J. Biomed. Mater. Res. 23 (1989) 417.
[2] E. Sheha, H. Khoder, T.S. Shanap, M.G. El-Shaarawy, M.K. El Mansy, Opt.-Int. J. Light Electron Opt. 123 (2012) 1161.
[3] M. Angelopolous, A.J. Epstein, A.G. MacDiarmid, F. Zuo, Phys. Rev. B 39 (1989) 3570.
[4] M.V. Kulkarni, A.K. Viswanath, Eur. Polym. J. 40 (2004) 379.
[5] M.I. Vladu, J.W. Fergus, Synth. Met. 156 (2006) 1401.
[6] M.A. Ali, E. Saion, N. Yahya, A. Kassim, K.M. Dahlan, S. Hashim, J. Eng. Sci. Technol. 2 (1) (2007) 111.
[7] J. Bhadra, D. Sarkar, Bull. Mater. Sci. 33 (5) (2010) 519.
[8] J. Bharda, D. Sarkar, Indian J. Pure Appl. Phys. 48 (2010) 425.
[9] R.A. Sharma, D. D'Melo, S. Bhattacharya, L. Chaudhari, S. Swain, Trans. Electr. Electron. Mater. 13 (1) (2012) 31.
[10] B.M. Novak, Adv. Mater. 5 (1993) 422.
[11] M.H. Blees, G.B. Winkelman, A.R. Balkenende, J.M.J. Den Toonder, Thin Solid Films **359** (1) (2000) 1.
[12] S. Zhou, L. Wu, J. Sun, W. Shen, Progress Org. Coat. 45 (1) (2002) 33.
[13] H.J. Song, Z.Z. Zhang, X.H. Men, Appl. Phys. A 91 (1) (2008) 73.
[14] J.B. Bharathibai, D. Kumar, ISRN Nanotechnoly, vol. 2011, 2011, 6pp. (Article ID 10.5402/2011/803910).
[15] H.J. Song, Z.Z. Zhang, X.H. Men, Eur. Polym. J. 43 (10) (2007) 4092.
[16] D. Lingaraju, K. Ramji, M.P. Devi, U.R. Lakshmi, Bull. Mater. Sci. 34 (4) (2011) 705.
[17] Y.C. Ching, Y.C. Ching, I.I. Yaacob, J. Comput. Theor. Nanosci. 9 (9) (2012) 1161.
[18] Y.C. Ching, Y.C. Ching, I. Yaacob, Mater. Technol. 27 (1) (2012) 113.
[19] S. Honmute, A. Lagashetty, A. Venkataraman, Indian J. Appl. Res. 3 (8) (2013) 91.
[20] D.B. Dupare, M.D. Shirsat, A.S. Aswar, Int. J. Res. Eng. Technol. 2 (12) (2013) 308.
[21] N. Gharehbash, A. Shakeri, J. Am. Sci. 9 (4) (2013) 602.
[22] S. Maheswaran, B. Bhuvaneshwari, G.S. Palani, N.R. Iyer, S. Kalaiselvam, Res. J. Recent 2 (2013) 17.
[23] G. Nasar, M.S. Khan, U. Khalil, Pak. Mater. Soc. 3 (2) (2009) 67.
[24] M. Pattabi, B.S. Amma, K. Manzoor, Mater. Res. Bull. 42 (2007) 828.
[25] A.R. Subrahmanyam, V. Geetha, A. kumar, A. Alakanandana, J.S. Kumar, Int. J. Mater. Sci. 2 (1) (2012) 27.
[26] S. Rajendran, M. Sivakumar, R. Subadevi, Mater. Lett. 58 (2004) 641.
[27] M. Liu, L. Gan, L. Chen, D. Zhu, Z. Xu, Z. Hao, L. Chen, Int. J. Pharm. 427 (2012) 354.
[28] X. Tai, J.H. Ma, Z. Du, W. Wang, J.A. Wu, Powder Technol. 233 (2013) 47.
[29] M. Salami-Kalajahi, V. Haddadi-Asl, H. Roghani-Mamaqani, Science 19 (2012) 2004.
[30] L. Feng, L. He, Y. Ma, Y. Wang, Mater. Chem. Phys. 116 (2009) 158.
[31] A.M. El Sayed, S. El-Sayed, W.M. Morsi, S. Mahrous, A. Hassen, Polym. Compos. 35 (2014) 1842.
[32] A.M. Shehap, Egypt J. Solids 31 (2008) 75.
[33] A. Hassen A, A.M. El Sayed, W.M. Morsi, S. El-Sayed, J. Appl. Phys. 112 (2012) 093525.
[34] N. Reddeppa, A.K. Sharma, V.V.R.N. Rao, W. Chen, Microelectron. Eng. 112 (2013) 57.
[35] W.E. Mahmoud, Euro. Polym. J. 47 (2011) 1534.
[36] W.E. Mahmoud, A.A. Al-Ghamdi, F. Al-Agel, Polym. Adv. Technol. 22 (2011) 2055.
[37] W.E. Mahmoud, W. Shirbeeny, A.A. Al-Ghamdi, S. Al-Heniti, J. Appl. Polym. Sci. 125 (2012) 339.
[38] R. Wen, L. Wang, X. Wang, G.H. Yue, Y. Chen, D.L. Peng, J. Alloy. Compd. 508 (2010) 370.
[39] K.R. Mohan, V.B.S. Achari, V.V.R.N. Rao, A.K. Sharma, Polym. Test. 30 (2011) 881.
[40] P.C. Sekhar, P.N. Kumar, U. Sasikala, V.V.R.N. Rao, A.K. Sharma, Eng. Sci. Technol. Int. J. 2 (2012) 908.
[41] F. Urbach, Phys. Rev. 92 (1953) 1324.
[42] S.K. O'Leary, S. Zukotynski, J.M. Perz, J. Non-Cryst. Solids 210 (1997) 249.
[43] I.S. Yahia, A.A.M. Farag, M. Cavas, F. Yakuphanoglu, Superlatt. Microstruct. 53 (2013) 63.
[44] A. Hassen A, S. El-Sayed, W.M. Morsi, A.M. El Sayed, „ J. Adv. Phys. 4 (3) (2014) 571.
[45] W. Sellmeier, Ann. Phys. Chem. 143 (1871) 271.
[46] S.H. Wemple, M. DiDomenico, Phys. Rev. B 3 (1970) 1338.
[47] B.J. Zheng, J.S. Lian, L. Zhao, Q. Jiang, Appl. Surf. Sci. 253 (2010) 2910.
[48] S. Ramesh, H.M. Ng, R. Shanti, K. Ramesh, Polym.-Plast. Technol. 52 (14) (2013) 1474.
[49] M.F. Mostafa, A. Hassen, Phase Transit. 79 (2006) 305.
[50] A.E. Kotp, Int. J. Basic Appl. Sci. 10 (2) (2010) 20.
[51] J.C. Dyre, T.B. Schroder, Rev. Mod. Phys. 72 (2000) 873.
[52] A.K. Jonscher, Nature 267 (1977) 673.
[53] W. Rehwald, H. Kiess, B. Binggeli, Z. Phys. B 68 (1987) 143.
[54] A.K. Jonscher, Dielectric Relaxation in Solids, Chelsea Dielectric Press, London (1983) 340.
[55] S. El-Sayed, K.H. Mahmoud, A.A. Fatah, A. Hassen, Physica B 406 (2011) 4068.
[56] G.E. Pike, Phys. Rev. B 6 (1972) 1572.